Int. J. Heat Mass Transfer. Vol. 19, pp. 751–756. Pergamon Press 1976. Printed in Great Britain

THE INTERACTION OF UNEQUAL LAMINAR PLANE PLUMES

BENJAMIN GEBHART,* HUSSAIN SHAUKATULLAH† and LUCIANO PERA‡
State University of New York at Buffalo, Parker Engineering Building, Buffalo, NY 14214, U.S.A.

(*Received* 18 *February* 1975 *and in revised form* 17 *September* 1975)

Abstract—Interactions between unequal laminar natural convection plumes generated by line heat sources were experimentally investigated using a Mach–Zehnder interferometer. These nominally free boundary flows were found to be affected by the presence of other similar flows which interfere with the supply of entrainment fluid. A model, based on the nature of the interacting flows, is successful in interpreting the mechanism.

NOMENCLATURE

f, stream function;
g, gravitational acceleration;
G, $4[Gr_x/4]^{1/4}$;
Gr_x, $\frac{gx^3}{\nu^2}\beta(t_0-t_\infty)\cos\theta$;
G_Q, $\left(\frac{gs^3}{\nu^2}\frac{\beta Q}{k}\right)^{1/5}$
h, merging height, see Fig. 4;
H, h/s;
I, thermal flux integral;
L, plume span;
M, see equations (7), (8) and (9);
N, temperature decay rate;
p, static pressure;
P, see equation (7);
Q_1, Q_2, plume strength, per unit span;
s_1, s_2, spacing;
t, local temperature;
t_0, plume midplane temperature;
t_∞, ambient medium temperature;
u, velocity component along the plume;
U, vertical velocity induced by entrainment;
v, velocity component across the plume;
V, plume entrainment rate;
x, distance along the plume from the plume source;
y, distance out from plane of plume symmetry.

Greek symbols

β, coefficient of thermal expansion;
η, similarity variable;
θ_1, θ_2, plume inclination, from vertical;
ρ, fluid density;
ψ, stream function.

INTRODUCTION

FREE-BOUNDARY buoyant flows are common in technology and in the environment. When these flows occur multiply they interact and the consequences thereof are of interest. An experimental study was carried out to investigate such an interaction between pairs of plane plumes. Pera and Gebhart [1] consider the interaction between laminar plumes of equal strength. Here results for the unequal plumes are presented. Review of related literature is given in Pera and Gebhart.

THE EXPERIMENTS

The plumes were generated by electrically heating nichrome wires about 18 cm long and 0.25 mm in diameter in an isolated enclosure of dimensions $69 \times 69 \times 84$ cm high. The strength of one of the plumes Q_1 was always 72 W/m while the strength of the other Q_2 was varied from 1.3 to 72 W/m in eight steps. For each Q_2, the spacing between the two wires was varied from 8.59 to 1.42 cm in six equal steps of about 1.42 cm. A 20 cm Mach–Zehnder interferometer was used to visualize the temperature field above the heat sources.

Characteristic results are seen in Figs. 1–3. In all photographs the left plume is stronger, with a strength of 72 W/m. Six spacings are seen in Figs. 1 and 2. In Fig. 1 the ratio of plume strengths Q_2/Q_1 is 0.019 and this is the smallest ratio studied. The stronger plume is hardly affected by the presence of the weaker one, even at small spacing. In Fig. 2 the ratio Q_2/Q_1 is 0.63 and is the largest ratio for unequal plumes. There is large effect on the stronger one. As the spacing is decreased, inclination increases and the plumes merge within a shorter distance. Figure 3 shows the effect a smaller plume on a larger one when the strength of the weaker plume is varied at a fixed spacing. As the ratio Q_2/Q_1 increases the stronger plume tilts more and more.

ENTRAINMENT PREDICTION OF INTERACTION

These experiments, along with those in [1], suggest that the basic mechanism in interaction is the limitation or restriction of the induced external inviscid flow, up between the plumes. This flow supplies their downstream entrainment. The restriction increases the induced flow velocity and causes an appreciable pressure inhomogeneity in the external field. This is balanced, across the plume, by the component of the buoyancy force normal to the principal flow direction. A model

*Professor of Mechanical Engineering, State University of New York at Buffalo, Buffalo, NY 14214.
†Graduate Research Assistant, Cornell University, Ithaca, NY 14853, U.S.A.
‡Engineer, FIAT Direzione Ricerca, Torino, Italy.

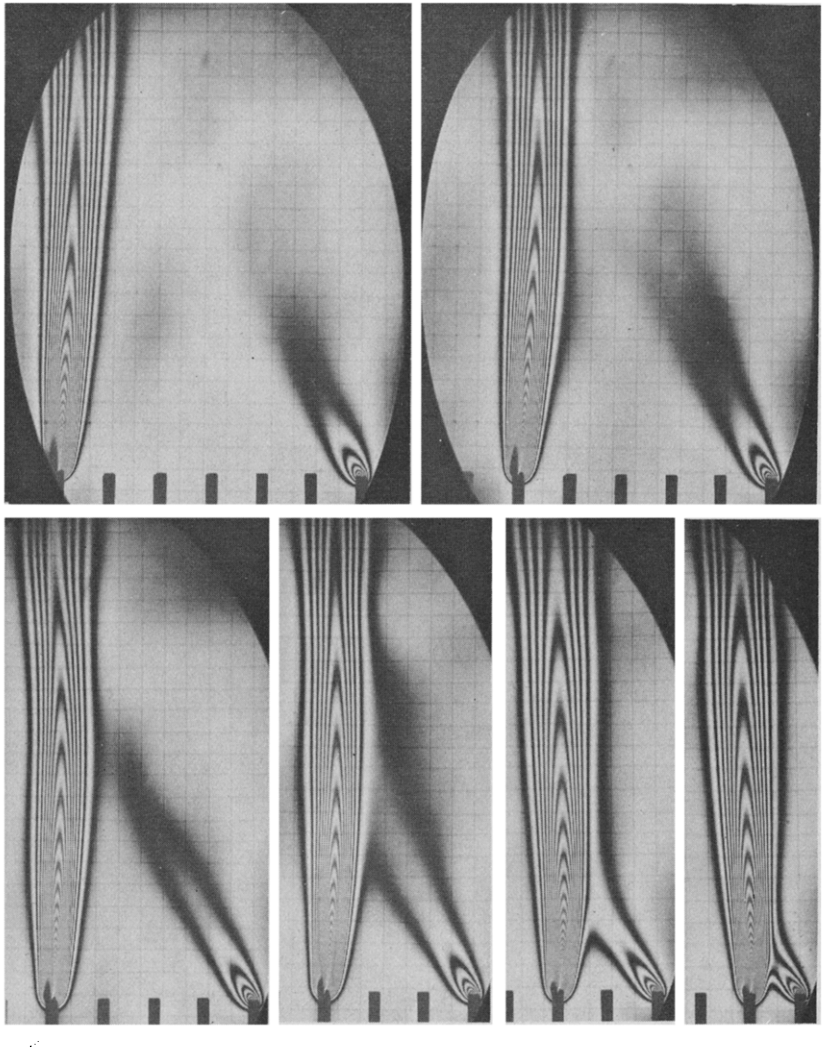

FIG. 1. Flow interaction between unequal-strength plane plumes. Wire length 18 cm, distance between grid lines 0.64 cm. Distance between sources are: 8.59, 7.16, 5.72, 4.29, 2.87 and 1.42 cm respectively. Heat dissipated in wires is 72 and 1.3 W/m respectively.

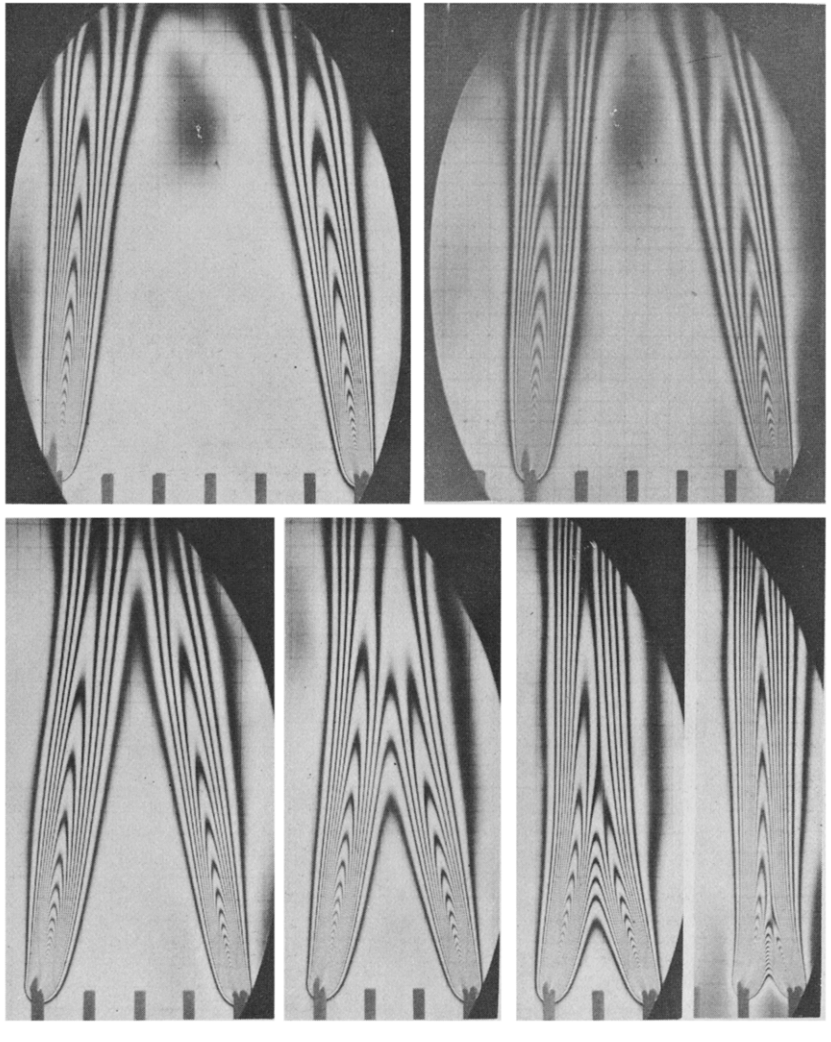

FIG. 2. Heat dissipated in wires is 72 and 46 W/m respectively. Other conditions as in Fig. 1.

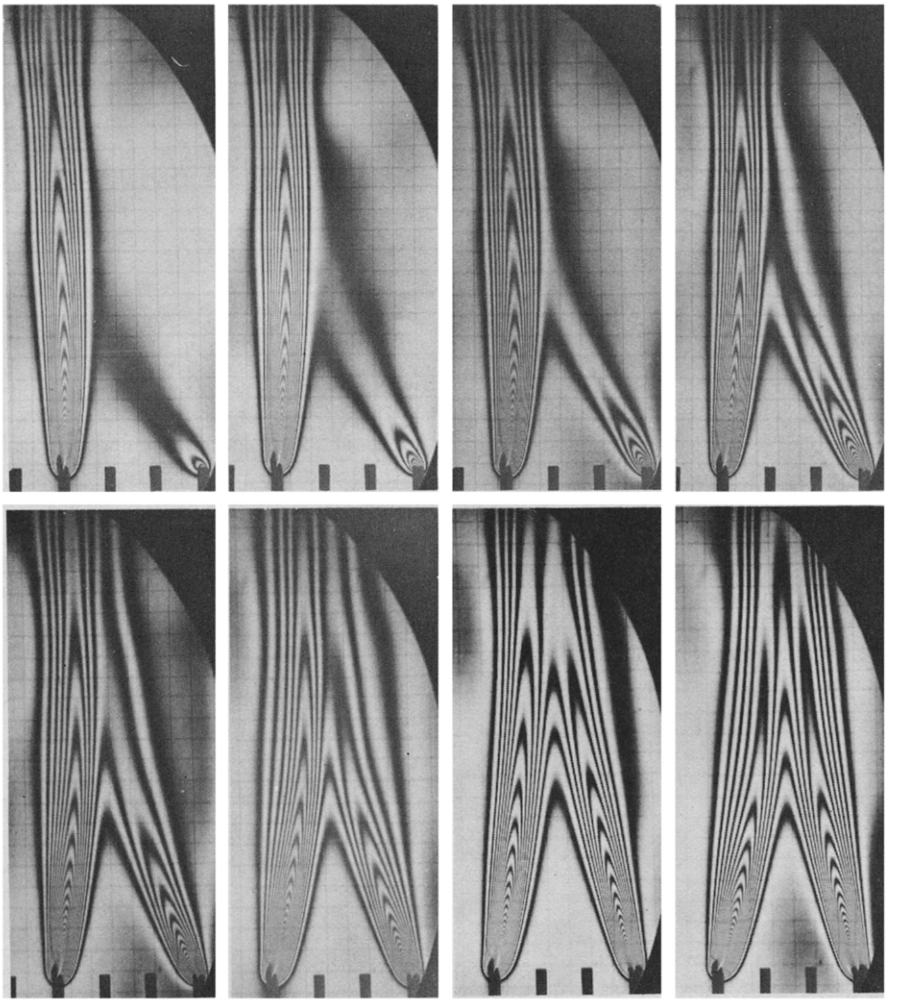

FIG. 3. Distance between sources 2.87 cm. Heat dissipated in left wire 72 W/m. Heat dissipation in right wire 1.3, 3.0, 5.3, 12, 21, 32, 46 and 72 W/m.

was developed for the interaction. The parameters are defined in Fig. 4. Bernoulli's equation relates the induced flow of velocity U, in the region between the plumes, to the difference between the motion pressure there, p_i, and the pressure in the ambient external medium, p_∞. This pressure difference is equated to the cross-plume buoyancy force component. Then, through continuity considerations, U is related to the entrainment rate required by each plume on the side of interaction. This model, successful for equal plumes, is here applied to unequal ones.

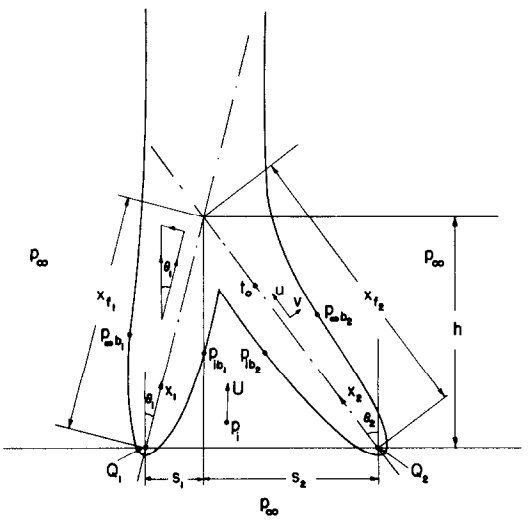

FIG. 4. Plane plume interaction for unequal strength plumes.

The inclined plumes are treated as vertical ones with the buoyancy force, $g\rho\beta(t-t_\infty)$, in the Grashof number Gr_x, reduced by the cosine of the angle between the vertical and plume centerline. The use of the boundary layer similarity formulation for these inclined plumes appears justified from two separate considerations. First, we can see in Figs. 1–3 that the inclined plumes, especially those at the larger spacings, have essentially straight centerlines. Second, the measured downstream decay of midplane temperature t_0-t_∞ was found to be approximately as $x^{-3/5}$, as predicted by analysis for vertical plane plumes and corroborated through measurements, e.g. by Schorr and Gebhart [2]. However, measured temperature levels are always appreciably lower than those calculated.

The similarity transformation for the plane plume, from Gebhart, Pera and Schorr [3], with the above modification, is:

$$u=\psi_y,\ v=-\psi_x,\ \psi=\nu G f(\eta),\ \phi(\eta)=\frac{t-t_\infty}{t_0-t_\infty},\ \eta=\frac{G}{4x}y$$

$$G=4\sqrt[4]{\left(\frac{Gr_x}{4}\right)},\quad Gr_x=\frac{g\beta(t_0-t_\infty)x^3\cos\theta}{\nu^2}$$

$$t_0-t_\infty=Nx^{-3/5},\quad N=\frac{1}{4}\left[\frac{Q^4}{\rho^4 c_p^4\nu^2 g\beta I^4\cos\theta}\right]^{1/5},$$

$$I=\int_0^\infty f'\phi\,\mathrm{d}\eta.$$

The solutions, in terms of the stream and temperature functions f and φ, are known for many values of the Prandtl number, Pr.

Considering the stronger plume first, the local, at x_1, motion pressure difference immediately across the boundary region of the plume is denoted by $p_{\infty b_1}-p_{ib_1}$. This is taken to be the result of, or balance for, the cross-plume buoyancy component, $g\rho\beta(t_1-t_\infty)\sin\theta_1$, integrated across the boundary region. With boundary-layer approximations this becomes

$$\begin{aligned}\Delta p_{b_1}&=p_{\infty b_1}(x)-p_{ib_1}(x)\\&=2\int_0^\infty g\rho\beta(t_1-t_\infty)\sin\theta_1\,\mathrm{d}y_1\\&=\frac{\rho\nu^2}{8x_1^2}G_1^3\tan\theta_1\int_0^\infty\phi_1\,\mathrm{d}\eta_1\propto x_1^{-1/5}.\end{aligned}\tag{1}$$

The difference Δp_{b_1} differs from $\Delta p=p_\infty-p_i$ by the order of dynamic pressure characteristic of the normal velocity component of the fluid drawn in by the plume for entrainment, $v_1(\infty)$ on each side. Now the normal component of velocity is $-v_1(\infty)=(3\nu/5x_1)G_1 f(\infty)$. The equivalent dynamic pressure, compared to Δp_{b_1} becomes:

$$\frac{\rho[v_1(\infty)]^2}{2\Delta p_{b_1}}=\frac{36f^2(\infty)}{25G_1\tan\theta_1}\int_0^\infty\phi\,\mathrm{d}\eta.$$

For $1/G_1\tan\theta_1$ small we may neglect this difference and assume that $\Delta p_{b_1}\simeq\Delta p$. A similar argument applies for the right plume.

Both p_i and U are taken to be uniform across the space between the plumes, at any given height. We may write the Bernoulli equation for the inviscid induction of fluid from below as $\Delta p=p_\infty-p_i=\rho U^2/2$ and (1) becomes:

$$\frac{\rho U^2}{2}=\frac{\rho\nu^2}{8x_1^2}G_1^2\tan\theta_1\int_0^\infty\phi_1\,\mathrm{d}\eta_1\propto x_1^{-1/5}.$$

Now, applying the same consideration to the other plume, of different strength, we find:

$$\frac{G_1^2}{x_1^2}\tan\theta_1=\frac{G_2^2}{x_2^2}\tan\theta_2.\tag{2}$$

From above, $U\propto x_1^{-1/10}(=x_2^{-1/10})$. Given this weak variation with x, U is approximated by the average value from $x=0$ to the position of interaction, as follows:

$$\begin{aligned}\bar U&=\frac{1}{x_{f_1}}\int_0^{x_{f_1}}U(x)\,\mathrm{d}x\\&=\frac{10}{9}U_{x_{f_1}}=\frac{10\nu G_{f_1}}{18x_{f_1}}\sqrt{\left(G_{f_1}\tan\theta_1\int_0^\infty\phi_1\,\mathrm{d}\eta_1\right)}\end{aligned}\tag{3}$$

$$\begin{aligned}\bar U&=\frac{1}{x_{f_2}}\int_0^{x_{f_2}}U(x)\,\mathrm{d}x\\&=\frac{10}{9}U_{x_{f_2}}=\frac{10\nu G_{f_2}}{18x_{f_2}}\sqrt{\left(G_{f_2}\tan\theta_2\int_0^\infty\phi_2\,\mathrm{d}\eta_2\right)}\end{aligned}\tag{4}$$

where $G_{f_1}=G_{x_{f_1}}$ and $G_{f_2}=G_{x_{f_2}}$.

This estimate for $\bar U$ is used over the area across which the fluid to be entrained enters the between-plume region, $A=(s_1+s_2)(h+L)$, where L is the length of the plume and s_1, s_2 and h are as defined in Fig. 4. This is an over-estimate, since the plume thickness is neglected. The flow rate, $\bar U A$, supplies the combined entrainment by the two plumes on their inside faces, LV, and we have:

$$\begin{aligned}LV&=-L\left(\int_0^{x_{f_1}}v_1(\infty)\,\mathrm{d}\eta_1+\int_0^{x_{f_2}}v_2(\infty)\,\mathrm{d}\eta_2\right)\\&=\nu Lf(\infty)(G_{f_1}+G_{f_2})\\\bar U A&=(s_1+s_2)(h+L)\bar U=\nu Lf(\infty)(G_{f_1}+G_{f_2}).\end{aligned}\tag{5}$$

From (3) and (4) we have:

$$G_{f_1}=G_{f_2}\sqrt[3]{\left(\frac{x_{f_2}\tan\theta_1}{x_{f_1}\tan\theta_2}\right)}.\tag{6}$$

Using (3) and (6) in (5), we obtain the following relation between $H_1=h/s_1$ and $H_2=h/s_2$.

$$\begin{aligned}&\frac{5}{9}\left(1+\frac{h}{L}\right)\frac{\left(\int_0^\infty\phi\,\mathrm{d}\eta\right)^{1/2}}{f(\infty)}(G_{f_1})^{1/2}\\&\qquad=(H_1)^{1/2}\frac{(H_1^2+1)^{1/2}}{\dfrac{H_1}{H_2}+1}\left[1+\sqrt[3]{\left(\frac{H_1(H_2^2+1)}{H_2(H_1^2+1)}\right)}\right].\end{aligned}$$

Now, G_{f_1} may be written in terms of a more convenient Grashof number, based on Q_1 and s_1 as defined below, to yield a simpler relation for the interaction.

$$\sqrt[5]{(Gr_{Q_1})}=\left(\frac{g\beta s_1^3 Q_1}{k\nu^2}\right)^{1/5}=G_{Q_1}$$

$$\begin{aligned}&\frac{5\sqrt{2}}{9}\left(1+\frac{h}{L}\right)\frac{\left(\int_0^\infty\phi\,\mathrm{d}\eta\right)}{f(\infty)}\left(\frac{1}{Pr\,I}\right)^{1/10}\sqrt{(G_{Q_1})}\\&\quad=P\left(1+\frac{h}{L}\right)\sqrt{(G_{Q_1})}\\&\quad=\frac{(H_1+H_1^3)^{2/5}}{\dfrac{H_1}{H_2}+1}\left[1+\sqrt[3]{\left(\frac{H_1(H_2^2+1)}{H_2(H_1^2+1)}\right)}\right]=M_1.\end{aligned}\tag{7}$$

The value of P depends only on the properties of fluid. From Gebhart *et al.* [3] we find $P=1.11$ for air, with Prandtl number of 0.7.

A similar equation may be obtained between G_{Q_2} and H_1 and H_2 if equation (4) is used in (5) and by eliminating G_{f_1} instead of G_{f_2}.

$$P\left(1+\frac{h}{L}\right)\sqrt{(G_{Q_2})} = \frac{(H_2+H_2^3)^{2/5}}{\frac{H_2}{H_1}+1}\left[1+\sqrt[3]{\left(\frac{H_2(H_1^2+1)}{H_1(H_2^2+1)}\right)}\right] = M_2. \quad (8)$$

If the ratio of (7) and (8) is taken, a relation between Q_1/Q_2 and H_1 and H_2 is obtained which is independent of fluid properties.

$$\left(\frac{Q_1}{Q_2}\right)^{0.1} = \left(\frac{H_1}{H_2}\right)^{0.3}\frac{(H_1+H_1^3)^{2/5}}{(H_2+H_2^3)^{2/5}} \times \frac{\left(\frac{H_2}{H_1}+1\right)\left[\sqrt[3]{\left(1+\frac{H_1(H_2^2+1)}{H_2(H_1^2+1)}\right)}\right]}{\left(\frac{H_1}{H_2}+1\right)\left[\sqrt[3]{\left(1+\frac{H_2(H_1^2+1)}{H_1(H_2^2+1)}\right)}\right]} = M_3. \quad (9)$$

Equation (7), for infinite span plumes, i.e. $h/L = 0$, is plotted in Fig. 5 in terms of $P\sqrt{(G_{Q_1})}$ vs M_1. The actual data are seen to have wide scatter and are about 50% below the prediction. The end-flow effect, $(1+h/L)$, is retained in Fig. 6. This brings most of the data closer to theory. About 58% of the points are within $\pm 25\%$ of it, but most are still lower. A similar scatter was found when equation (8) with G_{Q_2} was plotted vs M_2.

Equation (9) is plotted in Fig. 7. The data is again low. Some interesting trends are apparent, however. Recall that equation (9) is independent of fluid properties and that the analysis depends on both $1/G_2\tan\theta_2$ and $1/G_1\tan\theta_1$ being small compared to 1 and of the same order. For most of the experiments, $1/G_2\tan\theta_2$ was less than 0.07, whereas $1/G_1\tan\theta_1$ was between 2.85 and 0.04. To show the trends, four different symbols are used in Fig. 7, to separate the following classes of data.

I. $0.5 \leqslant \dfrac{1}{G_1\tan\theta_1}$, solid circles

II. $0.1 \leqslant \dfrac{1}{G_1\tan\theta_1} < 0.5$, open triangles

III. $0.05 \leqslant \dfrac{1}{G_1\tan\theta_1} < 0.1$, open circles

IV. $\dfrac{1}{G_1\tan\theta_1} < 0.05$, solid squares.

Clearly, as $1/G_1\tan\theta_1$ gets smaller the agreement between data and theory improves. Most of the data for points of type III and IV is within 10% of the theory. This trend is not found for the parameters used to plot Figs. 5 and 6.

The above model, used boundary layer results. These approximations apply for large Grashof number, for small boundary-layer thickness. For the data of this experiment the Grashof number,

$$G = 4\sqrt[4]{\left(\frac{g\beta(t-t_0)x^3\cos\theta}{4\nu^2}\right)}$$

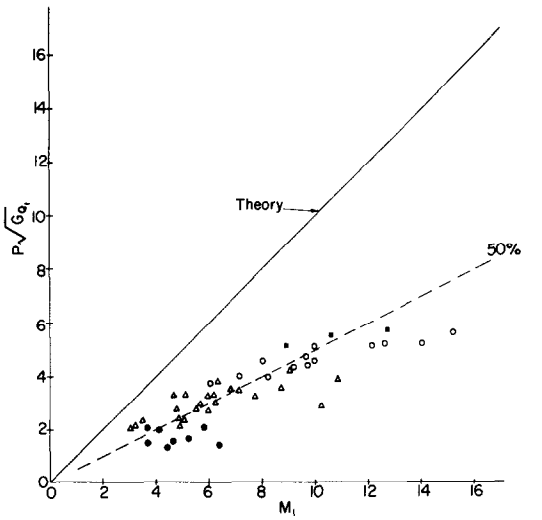

FIG. 5. Comparison of theory and data, without the end flow area effect $(1+h/L)$. ●, $0.5 \leqslant 1/G_1\tan\theta_1$; △, $0.1 \leqslant 1/G_1\tan\theta_1 < 0.5$; ○, $0.05 \leqslant 1/G_1\tan\theta_1 < 0.1$; ■, $1/G_1\tan\theta_1 < 0.05$.

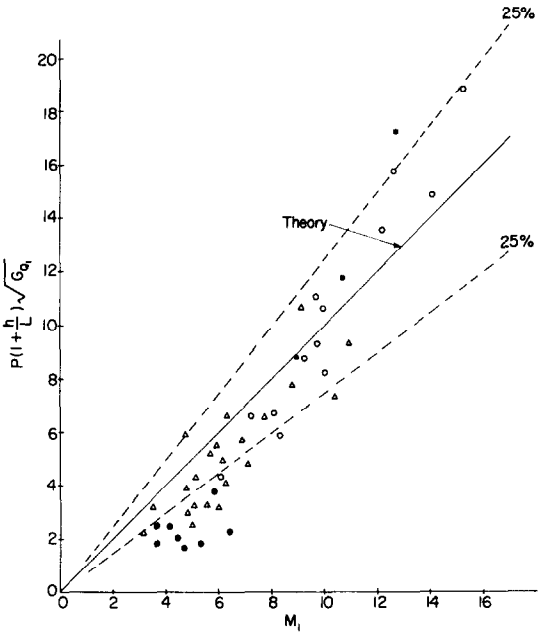

FIG. 6. Comparison of theory and data including the end flow area. Notations same as in Fig. 5.

ranges from 21 to 346. At the lower end of this range the agreement between the experiment and model would not be expected to be good. We also recall that the value of A is an overestimate of the actual area, since the plume thickness is neglected.

CONCLUSIONS

The postulate of the influence of the entrainment mechanism appears also to be supported for unequal plumes interaction. Disagreements are related to approximations made in the analysis. Much of the scatter in the data may be due to observed unsteadiness in these kinds of flows. Although the experiments were done in a large isolated enclosure, it was found that even a single plume was not exactly vertical, showing some sort of interaction.

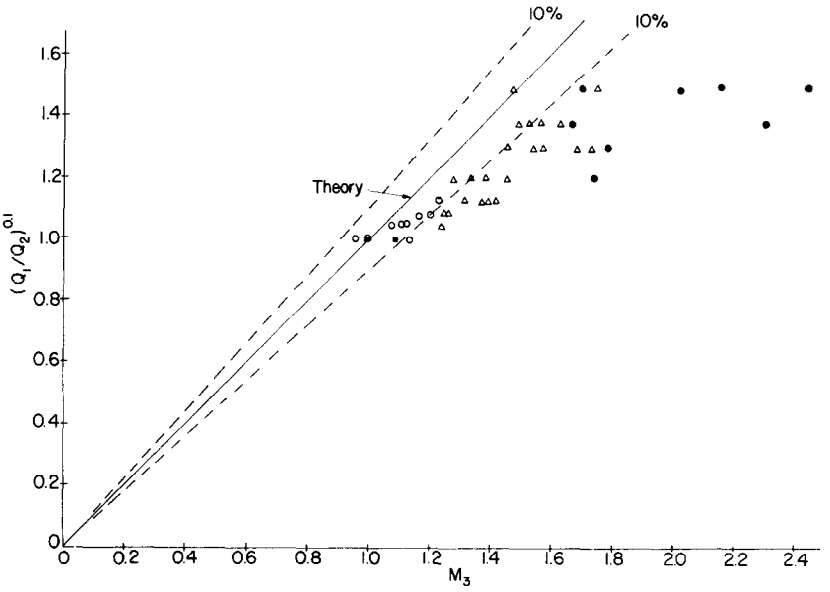

FIG. 7. Comparison of theory and data using equation (9). Notations same as in Fig. 5.

The experiments reported here were mainly intended for visualization of interaction. The Mach–Zehnder interferometer shows only the temperature field. For air ($Pr = 0.7$) the extent of the temperature field is approximately that of the velocity field and the plume seen corresponds to essentially the whole boundary layer flow field. To get a deeper understanding of the interaction a more detailed study of the outer inviscid flow field is necessary and future studies must be in the direction of visualization and measurement of this flow. Another important aspect of interaction is the effect of heat transfer. A step in this direction, for plume above or below a horizontal wall, has been taken recently by Reimann [4].

Acknowledgement—The authors wish to acknowledge financial support from the National Science Foundation under Research Grant GK-18529 for this research.

REFERENCES

1. L. Pera and B. Gebhart, Laminar plume interactions, *J. Fluid Mech.* **68**, 259–271 (1975).
2. A. W. Schorr and B. Gebhart, An experimental investigation of natural convection wakes above a line heat source, *Int. J. Heat Mass Transfer* **13**, 557–571 (1970).
3. B. Gebhart, L. Pera and A. W. Schorr, Steady laminar natural convection plumes above a horizontal line heat source, *Int. J. Heat Mass Transfer* **13**, 161–171 (1970).
4. J. Reimann, Experimental investigation of free convection flow from wires in the vicinity of phase interfaces, *Int. J. Heat Mass Transfer* **17**, 1051–1061 (1974).

INTERACTION ENTRE PANACHES LAMINAIRES PLANS DIFFERENTS

Résumé—Les intéractions entre différents panaches laminaires de convection naturelle et engendrés par des sources linéaires de chaleur, sont étudiées expérimentalement à l'aide d'un interféromètre Mach–Zehnder. Ces écoulements à frontière libre se trouvent être affectés par la présence d'autres écoulements semblables qui interférent avec l'apport du fluide d'entrainement. Un modèle, basé sur la nature physique des écoulements en intéraction, a permis d'interpréter les mécanismes avec succès.

GEGENSEITIGE BEEINFLUSSUNG IN UNGLEICHEN, LAMINAREN, EBENEN AUFTRIEBSSTRÖMUNGEN

Zusammenfassung—Die gegenseitigen Beeinflussungen in ungleichen, laminaren, natürlichen Auftriebsströmungen, wie sie an einer linienförmigen Wärmequelle entstehen, wurden experimentell untersucht in einem Mach–Zehnder-Interferometer. Die eigentlich freien Randströmungen wurden beeinflußt durch die Gegenwart anderer, ähnlicher Strömungen, die das verfügbare, zuströmende Fluid störten. Ein Modell, das der Natur der sich gegenseitig störenden Strömungen entspricht, erweist sich für die Interpretation der Vorgänge als erfolgreich.

ВЗАИМОДЕЙСТВИЕ НЕРАВНЫХ ПЛОСКИХ ЛАМИНАРНЫХ СТРУЕК

Аннотация — С помощью интерферометра Маха-Цендера экспериментально исследовались взаимодействия между неравными свободно-конвективными струйками, генерируемыми линейными источниками тепла. Найдено, что эти потоки с фактически свободными границами зависят от наличия других аналогичных потоков, которые интерферируют за счёт уноса жидкости. Модель, основанная на принципе взаимодействия потоков, успешно объясняет механизм процесса.